Energy 293 (2024) 130709

Contents lists available at ScienceDirect

Energy

journal homepage: www.elsevier.com/locate/energy

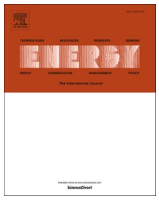

Design and optimization of a combined heat and power system with a fluidized-bed combustor and stirling engine

Wen-Lih Chen [a], Vadlakonda Sirisha [a], Chi-Yuan Yu [a], Yan-Ru Wang [a], Ming-Wei Dai [a], Janusz Lasek [b], Yueh-Heng Li [a,c,*]

[a] Department of Aeronautics and Astronautics, National Cheng Kung University, Tainan, 701, Taiwan
[b] Institute of Energy and Fuel Processing Technology, Zabrze, 41-803, Poland
[c] International Doctoral Degree Program on Energy Engineering, National Cheng Kung University, Tainan, 701, Taiwan

ARTICLE INFO

Handling editor: Krzysztof (K.J.) Ptasinski

Keywords:
Combined heat and power (CHP) system
Taguchi method
Stirling engine (SE)

ABSTRACT

In this study, a fluidized-bed biofuel system was integrated with a Stirling engine (SE) to create a combined heat and power (CHP) system with high energy efficiency. Methods for ensuring the stability of the SE and fluidized-bed combustion were investigated and implemented. The proposed design was tested experimentally, and the system successfully produced electricity from the heat of the flue gas generated during biomass combustion. The Taguchi method was employed to maximize the temperature of the fluidized bed by modifying three parameters: the sand height, air flow rate, and biomass feed rate. The biomass used in this study was discarded mushroom sawdust waste. The biomass feed rate was varied from 9.5 to 17 g/min, and the air flow rate was varied from 50 to 60 L/min. The integrated CHP system was found to yield 90−100 W of electric power and 1077.3 W of heat energy for producing hot water. The oxygen, carbon dioxide, carbon monoxide, and nitric oxide concentrations of the flue gas produced under the optimized system parameters were analyzed, and minimal emissions of carbon monoxide and nitric oxides, which are harmful gases, were discovered. In most experiments on SEs in the literature, liquid or gaseous fuels have been used to power the engine. However, this study successfully used solid biomass fuel to power a practical SE, thus widening the knowledge on the utilization of this renewable energy source for electricity generation. The results of this study indicate that the proposed CHP system is stable, clean, and efficient. This system potentially provides a solution for two problems, namely the disposal of mushroom sawdust waste and the eco-friendly generation of heat and electricity. Therefore, the proposed system is promising for green and sustainable power generation in the future.

1. Introduction

The widespread use of fossil fuels is a key factor contributing to the rising levels of atmospheric CO_2, which are exacerbating global warming and its adverse effects [1,2]. Reducing fossil fuel consumption and increasing energy efficiency are key strategies for reducing CO_2 emissions, such as using alternative fuels, like ammonia [3,4], hydrogen [4,5 [6]], and iron particles [7,8], and energetic oxidizers [9–12]. Fossil fuel consumption has been identified as a major cause of global warming, and this fact has prompted the international community to prioritize the transition toward renewable energy sources. Fossil fuels, including petroleum, are currently used to produce more than 20% of all primary energy used globally. The urgency of reducing fossil fuel consumption is evident from the devastating consequences of climate change, such as droughts, floods, forest fires, and other extreme weather events, which have caused infrastructure damage, property losses, and the deaths of people and animals. Several nations signed the Paris Agreement during the 2015 United Nations Climate Change Conference, pledging to take concrete action to reduce greenhouse gas emissions [13]. Consequently, alternative energy sources and methods for reducing the world's dependence on fossil fuels have attracted attention worldwide.

Biorefinery technology is a viable solution for reducing emissions. This technology can convert waste biomass into products such as biofuels [14,15], bio-oils, and synthetic gas (syngas) [16], thereby reducing waste accumulation and carbon emissions. The Paris Agreement states that accelerating the transition toward renewable energy sources is a fundamental strategy for combating climate change. Renewable energy is a sustainable and economically viable solution for preventing the adverse environmental consequences of fossil fuel consumption [17,18].

* Corresponding author. Department of Aeronautics and Astronautics, National Cheng Kung Univ., Tainan, 701, Taiwan.
E-mail addresses: yueheng@mail.ncku.edu.tw, yuehheng.li@gmail.com (Y.-H. Li).

https://doi.org/10.1016/j.energy.2024.130709
Received 15 September 2023; Received in revised form 13 December 2023; Accepted 13 February 2024
Available online 18 February 2024
0360-5442/

Nomenclature

M	Number of experiments at level L
m	Target value
n	Number of data points
P_{el}	Electric power output W
Q_f	Biomass feed rate g/min
$\overline{N_{\frac{S}{N}VE}}$	Mean S/N ratio in the nine relevant experiments
$s^2(x)$	Mean square error at sample point x
$(S/N)_{SB}$	S/N ratio for the STB approach
$(S/N)_{LB}$	S/N ratio for the LTB approach
$(S/N)_{NB}$	S/N ratio for the NTB approach
X	A set of samples
$x^{(n)}$	nth sample point
$\overline{X_L}$	Average S/N ratio
Y	A set of observations
$y^{(n)}$	nth observation
Y(x)	Observed responses
y_{min}	Minimum value among the observed responses
y_i	Value of a process or quality characteristic

Greek Symbols

$\eta_{overall}$	Overall efficiency of the CHP system
η_e	Thermal-to-electric efficiency
η_L	S/N ratio for an experiment performed at level L
μ	Mean

Abbreviations

CHP	Combined heat and power
DMSW	Discarded mushroom sawdust waste
FBC	Fluidized-bed combustor
HHV	Higher heating value
LPG	Liquefied petroleum gas
LTB	The larger, the better
NTB	The nominal, the best
SE	Stirling engine
S/N	Signal to noise
STB	The smaller, the better

Subscripts

el	Electric
f	Feed
L	Level

Biorefinery technology can be used to achieve innovative and sustainable waste management in rural agricultural communities [19,20]. This technology can also be employed to harness the potential of biomass waste and produce biofuels and bio-oils, which are renewable and low-carbon alternatives to fossil fuels. The conversion process in the aforementioned technology involves various thermal, chemical, and biological processes that efficiently transform biowaste into valuable energy sources. Moreover, biorefinery technology can be used to generate high-value products, such as biochemicals and bioplastics, thereby enhancing the economic viability of using biowaste for energy generation.

The adoption of biorefinery technology can bring several advantages to rural agricultural communities. First, this technology can provide an additional source of income by enabling the monetization of biomass waste, thereby boosting the local economy. Second, it reduces the environmental footprint and carbon emissions associated with biowaste accumulation. Third, the technology contributes to rural development by promoting sustainable practices and creating employment opportunities. However, to implement biorefinery technology, many challenges must be overcome, including technological limitations, infrastructure requirements, and the need for adequate policy support and financial incentives. Addressing these challenges is crucial for realizing the full potential of biorefinery technology in terms of its waste management and emissions reduction benefits. The aforementioned challenges can be addressed by employing a holistic approach that encompasses the implementation of advanced technologies, suitable support policies, and appropriate financial incentives. Research and collaboration among stakeholders are crucial for fully exploiting the potential of biorefinery technology and promoting sustainable development in rural areas.

Urgent measures must be adopted to address climate change, and enhancements in the efficiency of fossil fuel use can lead to considerable reductions in overall energy consumption and CO_2 emissions. Such reductions can be achieved using high-thermal-efficiency systems, specifically combined heat and power (CHP) systems [21]. Researchers have investigated CHP systems with various designs, including those with internal combustion (IC) engines, gas-turbine engines, Stirling engines (SEs), thermophotovoltaic arrays [22–24[25]], microreactors [6,26,27], or fuel cells as their prime mover. SEs may be the ideal prime mover for small-scale CHP systems, as indicated by the studies of Schneider et al. and Chen et al. [28–30]. CHP systems can be a sustainable solution for converting biowaste into electricity and heat while minimizing CO_2 emissions. These systems efficiently use rejected heat from thermodynamic cycles, thereby achieving lower greenhouse gas emissions for a given power output than that achieved by a conventional power system. Moreover, CHP systems are compact and inexpensive; thus, they are suitable for installation in remote or economically disadvantaged areas. Overall, recent advances in CHP technology have made CHP systems a promising option for large-scale sustainable energy generation.

Using solid biogenic fuels at the microscale to power simple systems is challenging [31,32]. For example, the gasification process, in which solid biomass is converted into syngas, is difficult to optimize. Combustion of syngas produces pollution, and syngas has low versatility, high powder content, and high soot load, which hinder its practical application [33,34]. Although microscale CHP systems can achieve a thermal-to-electric efficiency η_e of approximately 50%, researchers have focused on electricity generation techniques that involve IC engines because IC engine is a mature technology. IC engines can achieve η_e values of 22%–30% (a stand-alone η_e value of 30%–40%), whereas CHP systems that use exergy-based technologies, such as SEs, often have poor η_e values (e.g., 10%) [35]. However, SEs are much more flexible on fuel than IC engines. This is one of the key advantages of SEs over IC engines.

An SE is a heat engine that converts heat energy into mechanical energy through the expansion and contraction of a working gas. In SEs, the working gas transfers heat from a heat source to a heat sink. Conceptually, an SE closely resembles the ideal Carnot heat engine. An SE was first developed by Robert Stirling, and early SEs comprised air contained in cylinders and were commonly known as hot-air engines. However, modern SEs typically employ helium or hydrogen as the working fluid because of the superior heat absorption and release properties of these gases. To perform optimally, SEs require high temperature; thus, the efficiency of early SEs was limited by the materials available at the time.

Different SE configurations exist, such as the alpha, beta, gamma, and free-piston configurations. Most configurations comprise two moving parts: a power piston and a displacer piston. SEs operate in a sealed unit, which ensures that the working fluid is not leaking to the surrounding atmosphere. The movement of the displacer facilitates the cyclic flow of the working fluid. The working gas is initially in a hot chamber, which is maintained at a constant temperature by an external

heat source. Subsequently, the working gas progresses toward a cold chamber, where heat is extracted from the engine. This engine cycle is reversible; that is, a mechanically driven SE can also transfer heat energy from the cold end to the hot end, thereby effectively functioning as a refrigerator [36].

SEs with power outputs of 0.5–50 kW are commercially available. Low-power SEs have advantages over other engines with similar power output; for example, low-power SEs are less expensive to maintain because of their encapsulated roller bearings, which do not require oil lubrication. However, the maintenance process for SEs without oil-free mechanical transmission is relatively challenging [37]. SEs have high initial costs and may not be economically feasible; however, they can be viable for an integrated heat usage system and when the power demand is consistent [37,38].

Commercial SEs are predominantly solar-powered or gas-fired; little is known about the use of solid biofuels to power these engines. Fixed-bed combustors and fluidized-bed combustors (FBCs) are combustion systems commonly used for burning biomass. In fixed-bed combustion, the height of the solid bed is approximately constant, and gas flows slowly from the bottom of the solid bed to its top. By contrast, in fluidized-bed combustion, the solid bed is fluidized from underneath by using a regulated flow of air or gas. Fluidized-bed combustion has numerous benefits, including its adaptability to fuels with various characteristics, excellent thermal properties, and ability to combust biomass and agricultural residues efficiently, which results in low CO emissions and high carbon conversion rates at even small scales [39,40]. However, biomass with high alkali content can foul system components or cause the agglomeration of bed particles. To address these challenges, alternative bed materials must be adopted, and internal mixing techniques must be enhanced. To improve FBCs, various rapid fluidization methods that involve high gas velocities have been developed, including turbulent fluidization, bubbling fluidization, and rapid fluidized-bed combustion [41–43].

Bubbling fluidized-bed combustion is widely employed for burning solid fuels, including coal, biomass, and solid waste [43–45]. This process involves establishing a bed of solid particles, such as sand or limestone particles, within a combustor and fluidizing this bed by introducing a regulated flow of air or gas from below. In the present study, an SE was integrated with an FBC to achieve sustainable power generation and contribute to global efforts to combat climate change. The combination of the SE and FBC technologies holds considerable promise for increasing thermal efficiency [46–48] and reducing the emissions of CHP systems, thereby facilitating greener and more sustainable heat and power generation.

Few studies have investigated the performance of an SE integrated with an FBC. Urciuolo et al. [49] proposed a system that consisted of a γ-type SE and an FBC. In this system, the hot end of the SE is inserted inside the sand bed of the FBC to enhance the rate of heat transfer between the SE and the FBC. This configuration prevents the formation of a fouling layer on the heat-exchange pipes of the SE. The aforementioned system was found to generate electric power of up to 500 W, and its η_e value was 1.3%–2.2%. Schneider et al. [28] presented a CHP system with an integrated SE and FBC subsystem as the prime mover. In this subsystem, the hot end of the SE is inserted into the sand bed of the FBC for the same reasons as those reported in the study of Urciuolo et al. [49]. The SE adopted by Schneider et al. is an α-type SE, and its working gas can be pressurized up to 33 bars. The system of Schneider et al. was reported to generate electric power of up to 5.2 kW and have an η_e value of 14%–16%. The aforementioned two studies indicate that wood pellets can be used as fuel for an FBC and that inserting the SE directly into the FBC is a suitable configuration for an integrated SE–FBC system. The main objective of the present study was to develop a CHP system that has high efficiency and low CO_2 emissions and that can generate electrical and heat energy from biomass waste in a sustainable and eco-friendly manner. The CHP system designed in this study includes an integrated SE–FBC system that has a different configuration to the integrated systems developed by Schneider et al. and Urciuolo et al. [28,49]. The solid fuel used for the FBC of the designed system is discarded mushroom sawdust waste (DMSW). Therefore, the present study is expected to widen the knowledge regarding the use of solid biofuel for powering SEs. Disposal of DMSW is costly and produces greenhouse gases. At the time of writing, disposal of 1 ton of biomass waste costs the Environmental Protection Agency of Tainan City Government approximately 160 US dollars. This cost is expected to increase over time because of inflation. The CHP system proposed in this paper can be used to dispose of biomass waste at low cost and to generate revenue through the production of electricity and heat energy. Therefore, the proposed system is not only environmentally friendly but also financially attractive for farm owners and investors. Consequently, widespread application of the proposed green system can contribute to the mitigation of global warming.

2. Experimental equipment and process

2.1. Experimental setup and FBCs

Figs. 1 and 2 display a schematic and a photograph of the experimental setup, respectively. The designed system consists of a biomass fuel feeder, two FBCs, a twin-cylinder SE, an electricity generation system, an electricity control system, an inverter, and some common household appliances that consume power, such as LED light bulbs, electrical fans, and video players. Two combustors are required to supply heat to the twin-cylinder SE. Fig. 3 depicts a schematic of the FBCs, and Fig. 4 displays the upper and lower parts of these combustors. The fluidized bed has an outer diameter of 10 cm, an inner diameter of 9.3 cm, and a length of 50 cm. The fluidized bed comprises a rectification zone with an inner diameter of 9.3 cm and a length of 7.5 cm, and air can be injected into the combustor from this zone to fluidize sand. Biomass is injected above the rectification zone. A distributor plate with a diameter of 99 mm and an orifice diameter of 1 mm is placed above the rectification zone to distribute air flow evenly. As displayed in Fig. 3, each combustor's inner chamber contains sand for fluidization and rectifier beads for evenly distributing the air toward the distributor plate. The fluidization process occurs in the upper part of the two combustors. The upper and lower parts of the combustors are joined by screws, and a graphite plate is inserted between these parts to ensure tight sealing to prevent leakage. Moreover, a 99-mm-diameter distributor plate with 1-mm-diameter orifices is placed above the lower part of the combustors to distribute gas flow evenly into the upper part. The outward extrusions in the upper part of the combustors facilitate the insertion of thermocouples into the combustors for temperature measurements. In the experiments performed in this study, K-type thermocouples were used to measure the temperature at various positions within the combustors. Fig. 5 depicts the structure of the flue gas table used in this study. This table is placed above the combustors to hold the combustors and SE, and the table releases flue gas through its exhaust outlets. In this setup, the SE is placed on the outlet of the FBCs instead of inside the FBCs. This configuration offers several advantages over those adopted in Refs. [21,49]. First, embedding the engine within the fluidized bed would hinder scalability because of the complexity of installation and modification. The FBCs used in this study do not require complex installation; thus, their size can be conveniently reduced for small-scale applications. Second, if the SE's hot end were to be directly integrated with the sand in the fluidized bed, stringent structural and material designs would be required; SE installation is considerably more straightforward in the configuration adopted in this study. Third, in the adopted configuration, the hot end of the SE is not corroded by abrasive sand; thus, the service life of the SE is longer than it would be if the end did become corroded. Finally, the proposed configuration can be extended easily through the simple addition of SEs downstream of the flue gas pipe.

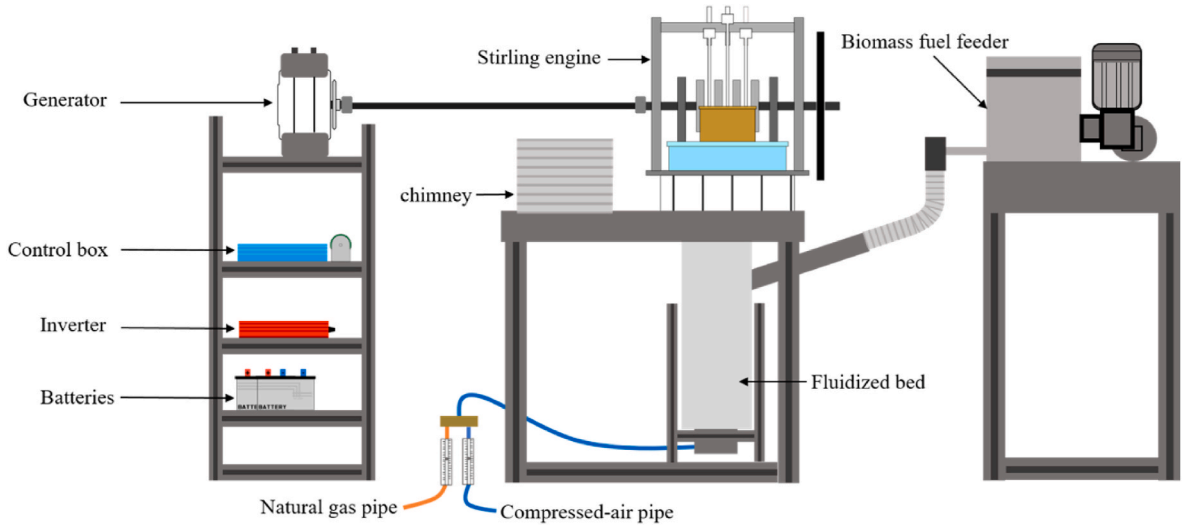

Fig. 1. Schematic of the designed system.

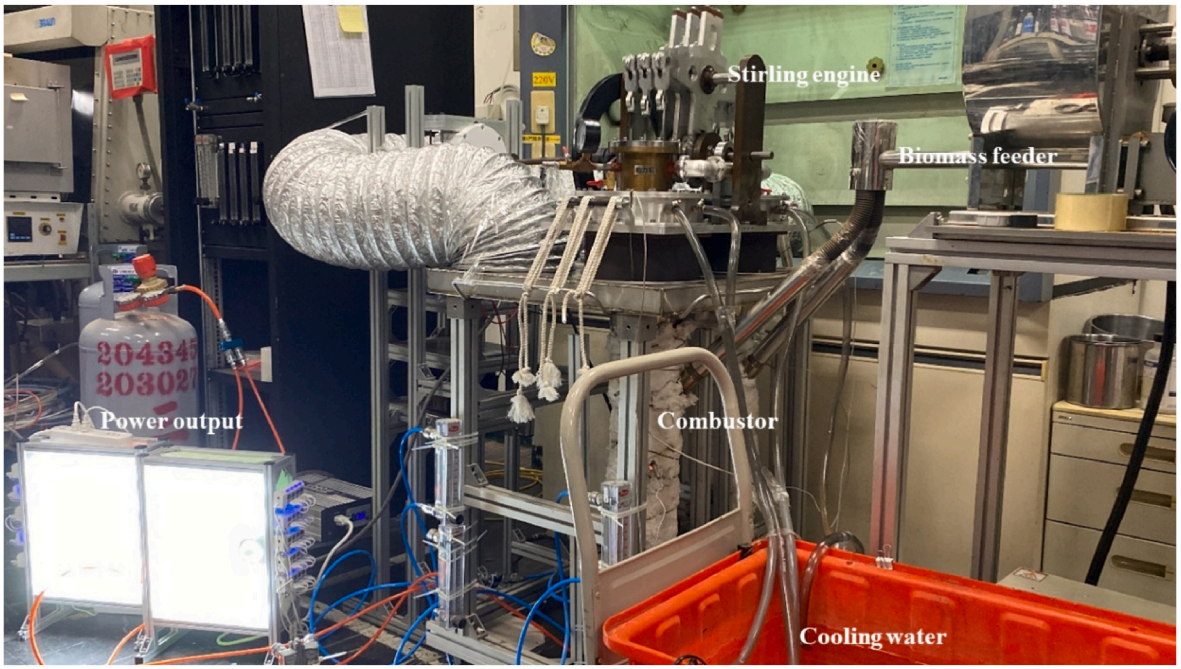

Fig. 2. Photograph of the experimental setup.

2.2. Stirling engine

Fig. 6 displays an engineering drawing and the configuration of the adopted pressurized two-cylinder SE with a medium temperature differential. The key dimensions and parameters of this SE are as follows: length = 500 mm, height = 450 mm, width = 320 mm, piston diameter = 100 mm, piston stroke = 68 mm, displacer cylinder diameter = 222 mm, displacer stroke = 48 mm, and phase difference between the two cylinders = 180°. A T-bar walking beam design is used to achieve a phase difference of 180° between the two cylinders, and this design enables a crank to be shared by the cylinders. The working gas of the SE is hydrogen pressurized to between 1 and 3 bar. The maximum engine speed is 600 rpm, and the maximum temperature of the hot end is approximately 550 °C. Fig. 7(a) displays the pressure gauge of the adopted SE. As depicted in Fig. 7(b), the SE is water-cooled, with cooling water being pumped from an external water tank by using two small pumps. Fig. 8(c)–8(e) presents the engine speed, shaft torque, and electric power of the adopted SE (373 rpm, 11.06 N-m, and 303 W, respectively) when hydrogen gas was pressurized to 2 bar and the temperature of the hot end was 450 °C. The aforementioned engine speed and shaft torque produced shaft power of 432 W (mechanical power), and the mechanical-to-electric efficiency of the power generation subsystem was 70% (obtained by dividing the electric power by the shaft power).

If biomass fuel is continuously supplied to its combustor, the SE can generate electricity without interruption. However, the consumption or addition of fuel can affect combustion, resulting in variation in the heating power supplied to the engine. This phenomenon causes changes in the temperature difference of the SE, which result in instabilities in its output power. To overcome this problem, a power generation unit that comprises a small 600-W wind turbine generator, two car batteries (combined voltage of 24 V), an inverter, and a control box is

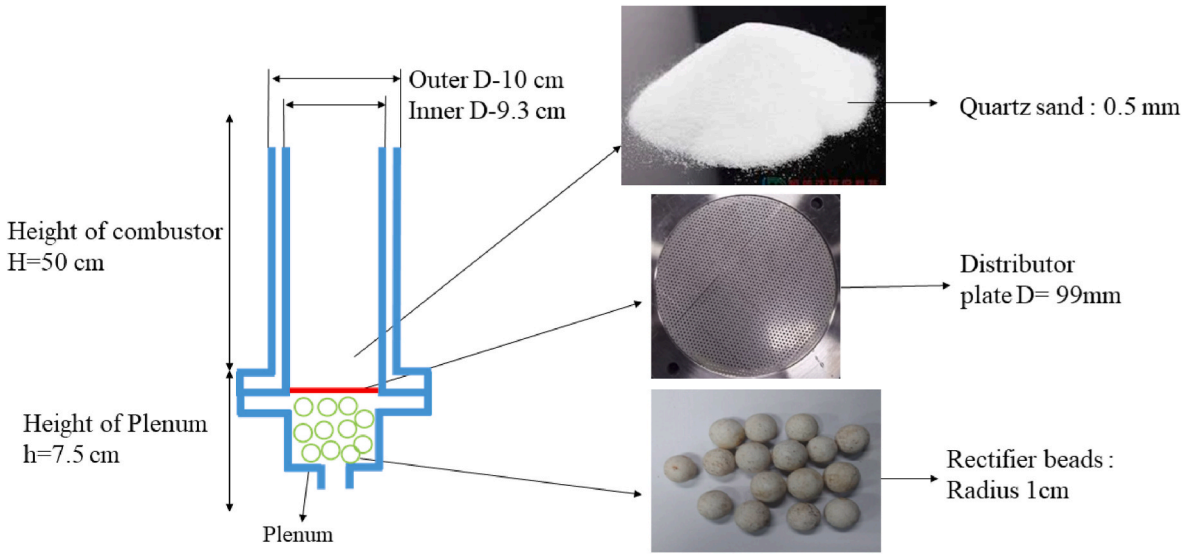

Fig. 3. Schematic of the FBCs and images of some of their internal components.

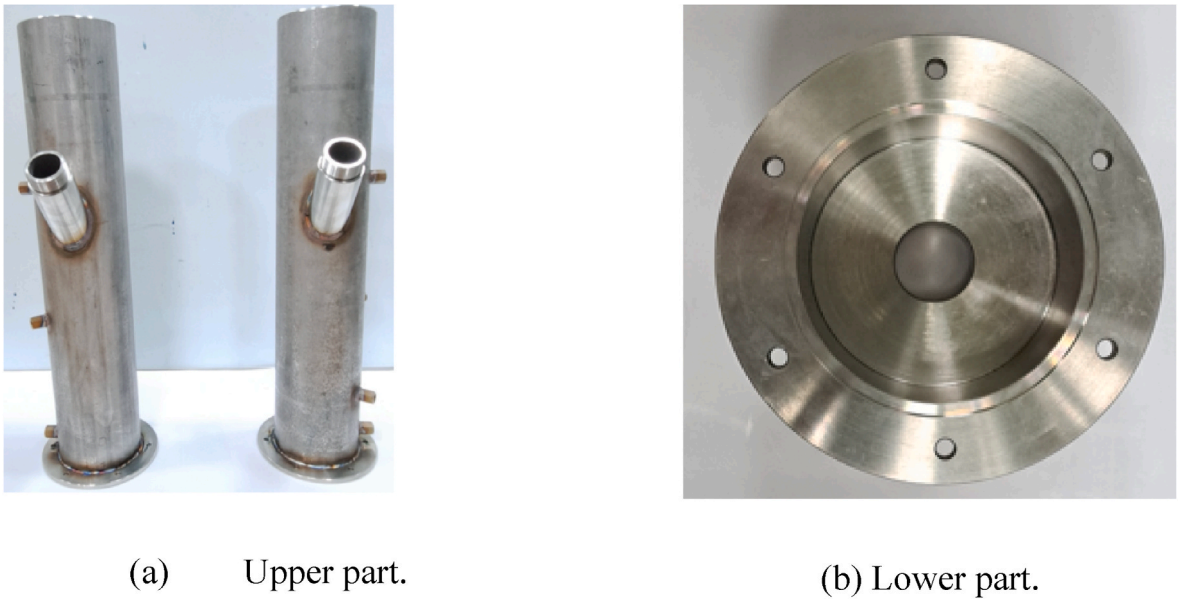

Fig. 4. Upper and lower parts of the FBCs.

incorporated into the proposed system (Fig. 8). The generator is driven by the SE, and the generated electric energy is stored in the batteries. The inverter then converts the 24-V DC electricity from the batteries into 110-V AC electricity for powering the household appliances. The flow of electricity between the generator, batteries, and inverter is managed by the control box. The large energy buffer of the batteries ensures stable output of power even when the SE is shut down temporarily.

2.3. Experimental procedure

In the present experiments, air was first injected at a rate of 50 L/min from the lower part of the combustor into the rectification zone of the reactor. Simultaneously, liquefied petroleum gas (LPG) was added to heat the sand. Once the sand had reached the desired preheating temperature, the LPG supply was stopped. Moreover, biomass was injected into the combustor to sustain the combustion process, resulting in fluidized-bed combustion. The SE was placed above the combustors and converted the thermal energy of the flue gas into mechanical energy. This mechanical energy then drove the generator, which resulted in the generation of electricity. The generated electric power and heating power were measured once the system had reached a steady state.

3. Optimization methodology

The following sections describe the methodology used in this study to identify the optimal operating conditions through the minimum number of tests.

3.1. Taguchi method

In the Taguchi method, the signal-to-noise (S/N) ratio, which is a quality evaluation standard, is used for analysis and optimization. This method enables optimization of a system through the minimum number of experiments. Desirable and undesirable outputs are referred to as “signal” (S) and “noise” (N), respectively. The Taguchi method can be implemented using three approaches, which are differentiated by the

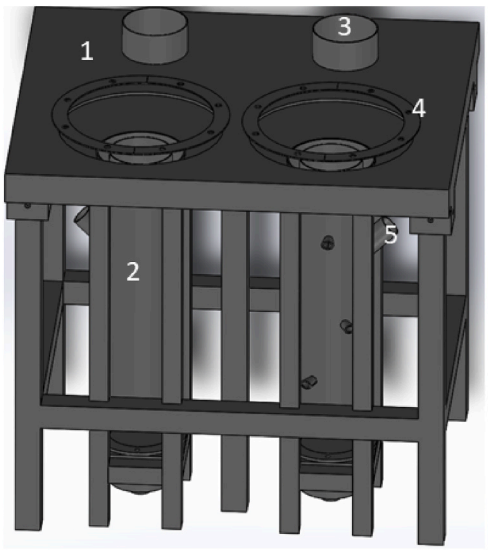

Fig. 5. Structure of the flue gas table and FBCs.

desired outcome: the smaller-the-better (STB), larger-the-better (LTB), and nominal-the-best (NTB) approaches [50].

In the STB approach, the value of the process or quality characteristic is minimized to a nonnegative ideal value that is typically 0. The STB approach can be used to obtain the yields of by-products and is expressed as follows:

$$\left(\frac{S}{N}\right)_{STB} = -10 \times \log\left[\frac{1}{n}\sum_{i=1}^{n} y_i^2\right] \tag{1}$$

In the LTB approach, the value of the process or quality characteristic is maximized. This approach can be employed to optimize product yield and is expressed as follows:

$$\left(\frac{S}{N}\right)_{LTB} = -10 \times \log\left[\frac{1}{n}\sum_{i=1}^{n} \frac{1}{y_i^2}\right] \tag{2}$$

In the NTB approach, the value of the process or quality characteristic is optimized to approach a predetermined target value as follows:

$$\left(\frac{S}{N}\right)_{NTB} = -10 \times \log\left[\frac{1}{n}\sum_{i=1}^{n} (y_i - m)^2\right] \tag{3}$$

where y_i is the value of the process or quality characteristic, n is the number of experiments in each set of the orthogonal array, and m is the target value.

An appropriate Taguchi method (the STB, LTB, or NTB method) can be employed to achieve optimization with the minimal number of experiments. The efficient combustion of biomass in an FBC is crucial for sustainable and environmentally friendly energy generation. To achieve optimal combustion performance, the temperature of the sand bed must be optimized. Therefore, the effects of factors that strongly influence the fluidization and combustion processes within the furnace were investigated. We focused on three crucial factors affecting the biomass combustion temperature: the sand height, air flow rate, and biomass feed rate.

The sand height in the fluidized bed influences the biomass combustion process because the sand is the major medium of heat transfer during this process. The height of the sand bed determines the heat distribution and circulation within the combustor and thus affects the overall combustion efficiency and temperature profile. An adequate sand height is required for ensuring efficient heat transfer from the bed to the biomass and thereby ensuring a favorable combustion rate and high thermal performance. The air flow rate is another key factor that strongly affects the combustion process in an FBC. Adequate air flow is essential for providing sufficient oxygen for biomass combustion, thereby facilitating complete and efficient burning. Moreover, the air flow rate influences the fluidization conditions within the combustor, that is, the mixing of sand particles and biomass; it thus strongly affects the overall combustion efficiency. The biomass feed rate also has a strong influence on the combustion process in an FBC. Biomass is the main fuel source for the combustion process inside a fluidized bed; thus, its feed rate directly affects the combustion rate and heat release. Appropriate control of the biomass feed rate ensures a consistent and uniform supply of fuel to the furnace, which minimizes fluctuations in temperature and ensures stable combustion conditions.

The goal of the optimization process conducted in this study was to identify the most favorable combination of the aforementioned three factors to achieve the required temperature conditions for biomass combustion. A range of experimental values was carefully selected for each factor. This range was determined by conducting preliminary experiments to understand the influence of each factor on the temperature profile. Table 1 lists the values selected for each factor for determining the optimal sand bed temperature. By optimizing the sand bed temperature, we aimed to improve the combustion efficiency and reduce emissions, thereby achieving cleaner and more sustainable energy generation.

An L9 orthogonal array was adopted to perform the optimization process (Table 2), and three levels were selected for each factor. The L9 orthogonal array enabled the systematic and efficient examination of the interactions between the three selected factors and their combined effect on temperature.

3.2. Combustion characteristics of biomass

3.2.1. Analysis of fuel properties

Table 3 presents the estimated calorific values of DMSW and Australian coal. The higher heating value (HHV) of the DMSW was 17.13 MJ/kg, which was marginally lower than that of the Australian coal (26.13 MJ/kg). This disparity in the HHV can be attributed to the higher fixed carbon fraction in the Australian coal, which was approximately 46 wt% higher than that in the DMSW. Conversely, the volatile matter content in the DMSW was nearly 76 wt% higher than that in the Australian coal; thus, the DMSW would be easier to ignite. Consequently, during combustion, the DMSW would burn primarily because of the presence of volatile matter, whereas the Australian coal would primarily undergo coke burning. Both fuel sources had ash content of approximately 15–19 wt%, which suggested that they had relatively high inorganic content. The sulfur content of the DMSW and Australian coal were 0.55 and 0.52 wt%, respectively. In summary, the DMSW and Australian coal had different calorific values, fixed carbon contents, volatile matter contents, ash contents, and sulfur contents. These differences resulted in them having different combustion behaviors and overall suitability.

4. Optimization of the combustion temperature

An increase in the sand bed temperature T_1 causes an increase in the power output. Therefore, the LTB approach was selected in this study. Each of the nine experiments to be performed was conducted twice. The S/N ratio was calculated for each experiment by using Eq. (2), and the results were averaged (Table 4).

$$\overline{X_L} = \frac{1}{M}\sum \eta_L \tag{4}$$

where X is factor A, B, or C; $\overline{X}_L$ is the average S/N ratio in each set of experiments for factor X at level L; M is the number of experiments at level L; and η_L is the average S/N ratio of level L for factor X. For example, the average S/N ratio of factor A at level 1 was calculated as

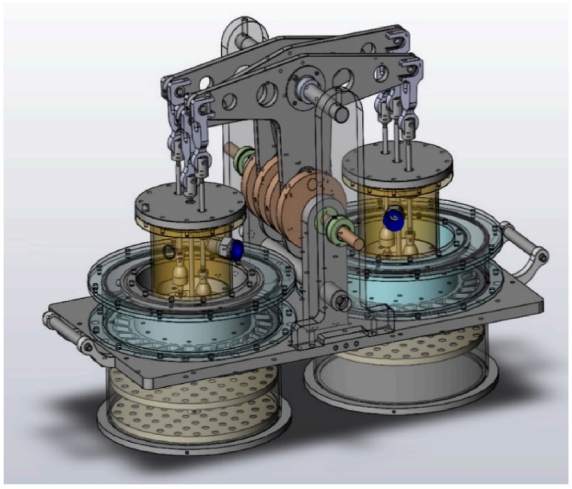

(a) Engineering drawing of the adopted SE.

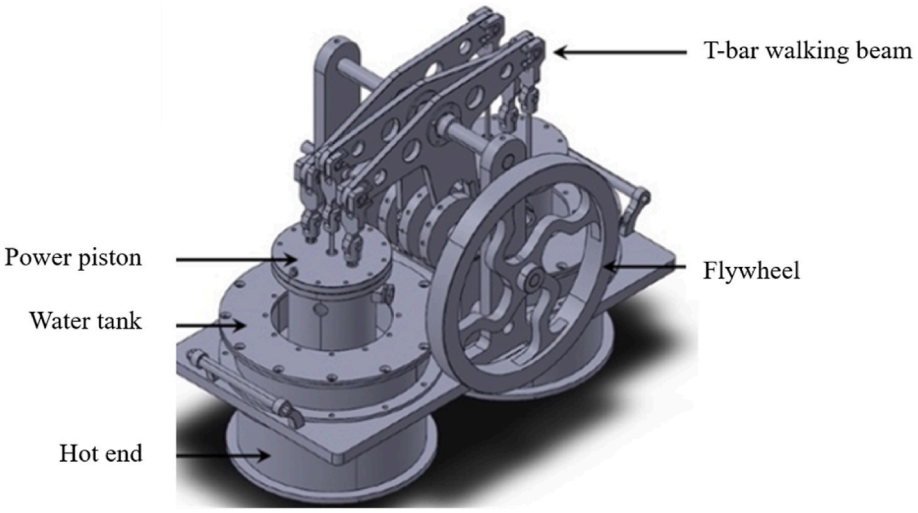

(b) Configuration of the adopted SE.

Fig. 6. Engineering drawing and configuration of the adopted 500-W SE.

follows:

$$\overline{A_1} = \frac{1}{4}(\eta_1 + \eta_2 + \eta_3 + \eta_4) \tag{5}$$

The S/N ratios for each level and factor are listed in Table 5. In this table, *Difference* represents the difference between the maximum and minimum S/N ratios of each factor, and *Rank* indicates the ranking of this difference. The optimal level for each factor was the level at which the highest S/N ratio was obtained. In the Taguchi method, the optimal S/N ratio is calculated as follows:

$$\frac{S}{N_{opt}} = \frac{S}{N_{AVE}} + \left(A1 - \frac{S}{N_{AVE}}\right) + \left(B1 - \frac{S}{N_{AVE}}\right) + \left(C3 - \frac{S}{N_{AVE}}\right) + \left(D2 - \frac{S}{N_{AVE}}\right) \tag{6}$$

where S/N_{AVE} (=56.74 in this study) is the mean S/N ratio in the nine sets of experiments; S/N_{OPT} is the predicted S/N ratio in the optimal experiment; and A1, B3, and C3 indicate the maximum S/N ratios of factors A, B, and C, respectively. The values of A1, B3, and C3 in this study were 57.97, 57.91, and 56.94, respectively (Table 5). The optimal parameters are listed in Table 6, and these parameters were validated by performing an experiment. The theoretical and experimental S/N ratios for the optimal parameters were 58.86 and 59.55, respectively (Table 7); thus, these ratios agreed favorably. The Taguchi investigation revealed that each considered factor strongly affected combustion and thus the temperature profile.

Specifically, an increase in the air flow rate and biomass feed rate improved fluidization, thereby enhancing combustion and increasing the furnace temperature. Conversely, a decrease in these rates hindered combustion, which resulted in unstable conditions and decreased the furnace temperature. For example, at a sand height of 6 cm and an air flow rate of 50 L/min, the bed temperature was approximately 693 °C,

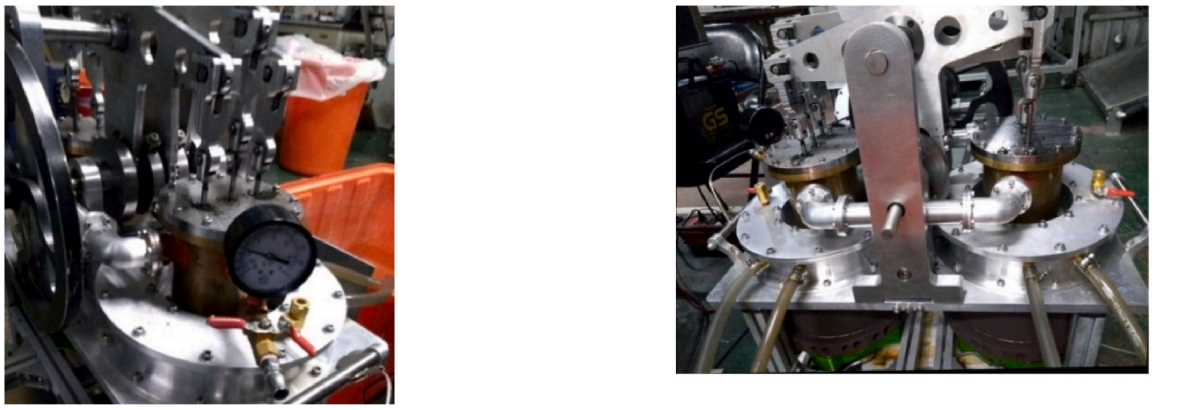

(a) Engine pressure gauge. (b) Cooling water recirculation pipes.

Fig. 7. Photograph of the adopted 500-W SE: (a) engine pressure gauge and (b) cooling water recirculation pipes.

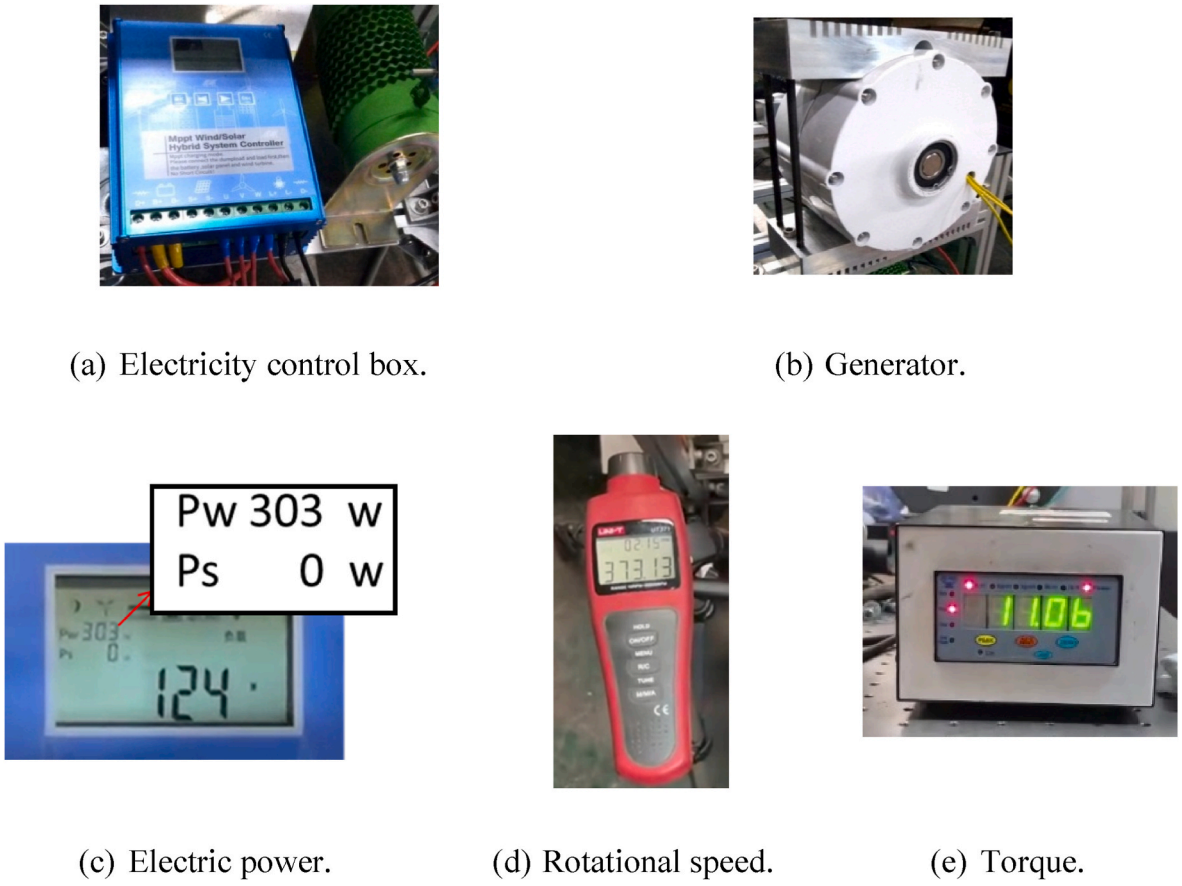

(a) Electricity control box. (b) Generator.

(c) Electric power. (d) Rotational speed. (e) Torque.

Fig. 8. (a) Electricity control box and (b) electric generator of the adopted SE. (c) Electric power, (d) rotational speed, and (e) torque readings obtained in an experiment performed with the SE.

Table 1
Factors and levels for the temperature experiment.

Level	Sand height (cm)	Flow rate of air (l/min)	Feed rate of biomass (g/min)
L1	2 [A1]	50 [B1]	9.5 [C1]
L2	4 [A2]	55 [B2]	13 [C2]
L3	6 [A3]	60 [B3]	17 [C3]

which suggested that a low air flow rate resulted in an insufficient supply of oxygen for biomass combustion, thereby causing combustion instability. By contrast, the maximum temperature (907.02 °C) was achieved using a sand height of 2 cm, a biomass feed rate of 17 g/min, and an air flow rate of 60 L/min. This parameter combination resulted in well-balanced fluidization and combustion processes with long-term stability. Therefore, the highest S/N ratio and thus highest combustion efficiency were achieved with this combination. Fig. 9 depicts the S/N ratios in the nine sets of experiments.

Table 2
L9 orthogonal array.

NO.	Sand height (cm)	Airflow rate (l/min)	Biomass feed rate (g/min)
1	2	50	9.5
2	2	55	13
3	2	60	17
4	4	55	9.5
5	4	60	13
6	4	50	17
7	6	60	9.5
8	6	50	13
9	6	55	17

Table 3
Proximate analysis of DMSW and Australian coal.

Proximate analysis of waste mushroom and Australian coal		
	Mushroom waste	Australian coal
Volatile matter	76.1	34.8
Fixed carbon	5.4	46.2
Ash	18.5	18.87
Elemental analysis (wt. %)		
C	43.90	73.3
H	5.53	4.16
N	29.29	5.26
O	2.23	1.15
S	0.55	0.53
Calorific value (MJ/kg)		
HHV	17.13	26.13

Table 4
S/N ratios for the nine sets of experiments.

NO.	Temperature (°C)	S/N ratio
1	693	56.81
2	744	57.43
3	907.02	59.15
4	706.06	56.97
5	685.4	56.71
6	558.14	54.13
7	782.6	57.87
8	597.12	55.52
9	642.05	56.15

Table 5
S/N response table for temperature.

Level	Sand height	Flow rate of air	Feed rate of biomass
L1	57.97	55.48	55.52
L2	56.05	56.85	56.55
L3	56.72	57.91	56.94
Max	57.97	57.91	56.94
Min	56.05	55.48	55.21
Difference	1.92	2.43	1.73
Rank	2	1	3

Table 6
Optimal combustion parameters determined using the Taguchi method for the maximizing combustion temperature.

Optimal experiment condition	Taguchi method
Sand height (cm)	2
Flow rate of air (l/min)	60
Feed rate of biomass (g/min)	17

The results of the experimental analysis provided valuable insights regarding the effects of the air flow rate, biomass feed rate, and sand height on the biomass combustion temperature in an FBC. These insights can be used to optimize the combustion process to increase the combustion temperature and combustion efficiency. Moreover, the insights enable the design and implementation of efficient and sustainable energy generation systems.

Table 7
Validation results for the optimal parameters.

Ratio	Taguchi method
Theoretical optimization S/N *ratio*	58.86
Experimental S/N *ratio*	59.55

4.1. Preheating and heating processes of the fluidized bed

Fig. 10 displays images of the fluidized bed at three temperatures, namely 200, 500, and 700 °C, during the CHP system's startup process. As the temperature in the combustor increased, the speed of the air molecules in the combustor also increased, which promoted bubbling and fluidization. The optimized parameters were used during preheating. The air flow rate was 45 L/min, and LPG was injected at a flow rate of 3–4 L/min to preheat the sand. The sand bed was heated slowly inside the combustor. As the temperature increased, bubbling fluidization intensified. The sand began moving vigorously, and the amount of heat transferred across the bed material increased. Once the bed temperature at 2 cm above the distributor plate (T1; Fig. 10) had reached 500 °C, biomass was injected into the combustor through the feeding hole. This hole was oriented at an angle of 45° with respect to the axis of the combustor. Biomass was fed into the combustor under gravity at an initial feeding rate of 8 g/min.

To reach the desired temperature, the air flow rate and biomass feed rate were then slowly increased. As the bed temperature increased, the variation in the fluidization conditions also increased. At 850 °C, which is higher than the ember temperature (i.e., 800 °C), the LPG supply was turned off, and DMSW was fed into the proposed CHP system. The fuel conversion process took approximately 10–15 min. After the fuel conversion, the temperature of the bed material gradually decreased to 675 °C. After approximately 8 min, the temperature increased again to 730 °C and slowly reached equilibrium, at which point the fuel conversion process concluded.

4.2. Temperature results for the designed CHP system

The optimized experimental parameters were used to operate the designed CHP system. Figs. 11 and 12 display the temperatures of the two combustors at various locations when they were connected to the SE. Specifically, T1 and T2 were the bed temperatures 2 and 8 cm above the distributor plate, respectively. These locations had similar temperatures, which indicated a uniform heat distribution in the fluidized bed. T3 represents the flame temperature measured 18 cm from the distributor plate, and T4 represents the temperature at the exit of the combustor, where the heat of the flue gas was transferred from the combustor to the bottom plate (hot end) of the SE.

After the sand had been preheated with LPG during the initial stage of biomass injection (0–700 s), the temperature fluctuated, and the biomass underwent volatile combustion. Once a temperature of 700 °C had been reached, the LPG supply was turned off, and the biomass combustion process stabilized. During this phase, the air flow rate was maintained at 55 L/min, and the biomass feed rate ranged from 12 to 13 g/min. The system then operated in a stable state for 30 min, during which the SE's bottom plate began to be heated gradually.

Subsequently, the feed rate was gradually increased to 17 g/min for both combustors, which resulted in the temperature increasing to 800–900 °C. Once the SE's plate temperature had reached 100–130 °C, the engine was started, and power generation began. The temperature of the SE's hot end increased to 260–270 °C, and the designed CHP system generated 90–100 W of electric power. This system then continuously

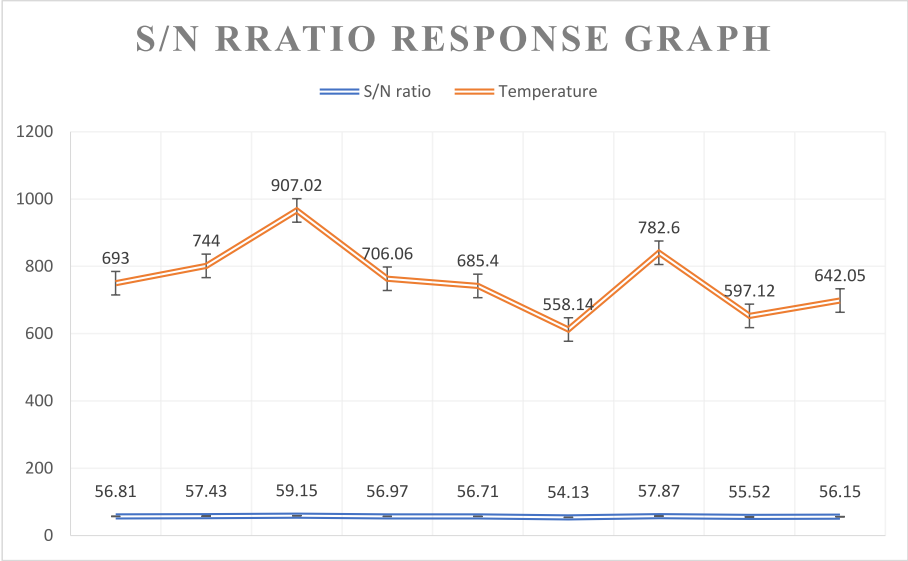

Fig. 9. S/N ratios in the nine sets of experiments.

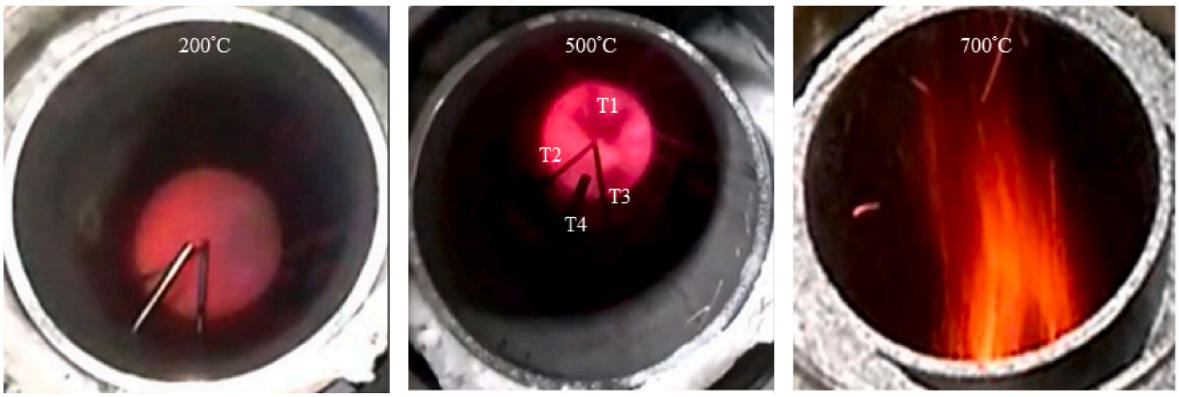

Fig. 10. Images of the fluidized bed at different temperatures.

and steadily operated for 1–2 h.

The flue gas temperature at the combustor outlet was strongly correlated with the biomass feed rate Q_f. Low feed rates of 11–13 g/min resulted in a stable flue gas temperature of approximately 730 °C. However, when the biomass feed rate was increased to 17 g/min, the temperature increased considerably to 800–900 °C. This temperature increase was attributable to the increase in the air flow, which effectively increased the combustion temperature. Consequently, the flue gas had higher energy when the feed rates were higher. An energy balance analysis performed for the bubbling fluidized-bed combustion chamber revealed that the additional energy provided by the increase in fuel was predominantly transferred to the flue gas. This was because of a reduction in the residence time of volatiles and unburnt gaseous species in the freeboard region located above the fluidized bed, which resulted in the combustion process and heat release primarily occurring in this area. Notably, these findings challenge the widely held assumption that higher fluidization velocities lead to greater heat release in bubbling fluidized-bed systems. Furthermore, although higher air preheating temperatures may improve the heat supply in the fluidized-bed area, they also result in greater energy transfer around the combustion chamber. However, the decoupled power of the SE did not increase proportionally with Q_f. The implications of this result are examined in a subsequent section discussing the performance and efficiency of the SE.

The combustion parameters directly affect the performance of the SE. To achieve heat transfer to the SE with maximum efficiency, meticulous attention should be paid to the design of the heat exchanger and the characteristics of the working fluid. The efficiency of heat transfer to the SE is strongly influenced by the coefficients of heat transfer within the fluidized bed, particularly in the upstream section of the bed. Alves et al. [51] reported a heat transfer coefficient of 280 W/m^2K for the transfer of heat generated through fluidized-bed combustion to an SE. Brown et al. [28] and Ghani et al. [52] investigated the relationship between the fluidization velocity and the heat transfer coefficient in a bubbling fluidized bed; they discovered a wide range of heat transfer coefficients: 250–480 W/m^2K. Various factors–such as the particle distribution, bubble growth, reactor and heat exchanger geometry, bed material temperature, and fluidization velocity—affect the heat transfer coefficient. The experimental data measured in this study were insufficient for determining the heat transfer coefficient; therefore, the heat transfer to the SE was estimated from the temperature at the hot end.

4.3. Power output results

The electric power output by the designed CHP system was primarily influenced by the temperature difference between the hot and cold ends of the SE. The hot end was maintained at 270 °C, and the cold end was maintained at room temperature by using a water–ice cooling system. The engine operated at a speed of 310 rpm when the temperature of the hot end was between 260 and 270 °C. Fig. 13 illustrates the relationship

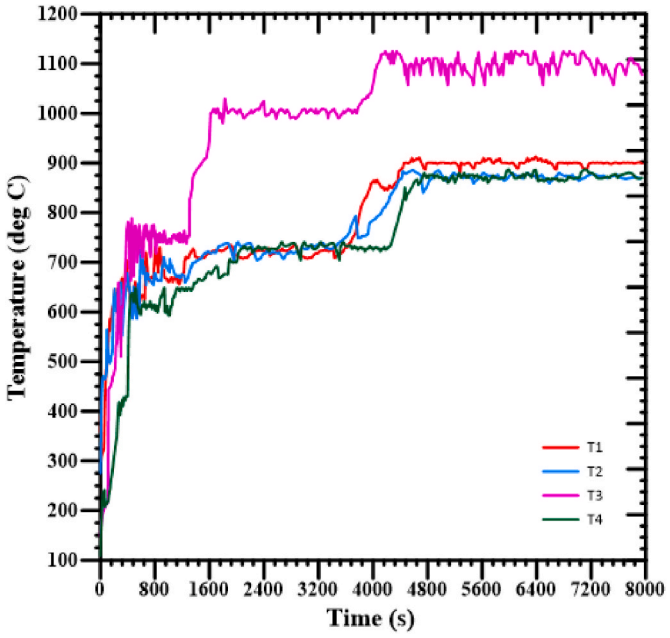

Fig. 11. Temperature of the first combustor during the startup of the designed CHP system.

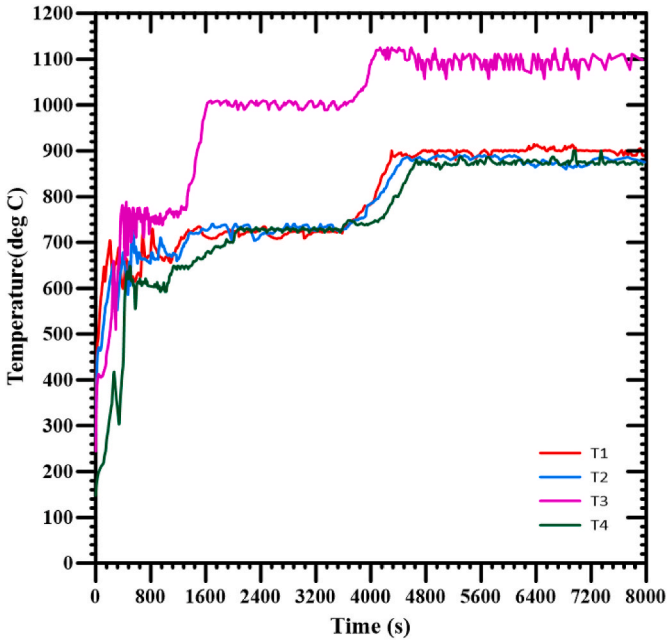

Fig. 12. Temperature of the second combustor during the startup of the designed CHP system.

between the electric power and fluidized-bed temperature for the designed system. The maximum electric power of 90–100 W was achieved at a fluidized-bed temperature of 900 °C. The temperatures of the combustor outlet and the SE's hot end were different because of various factors, such as the loss of heat to the cooling system, the escape of heat with the exhaust gas, and the dissipation of heat from the outer surfaces of the burner and table frames.

The calculation of the designed system's η_e value and overall efficiency $\eta_{overall}$ is detailed in the Appendix. Under the maximum electric power, the η_e and $\eta_{overall}$ values of the designed system were 2.04% and 24.2%, respectively. A comparison of the performance of the systems designed in this study and other studies is provided in Section 4.5.

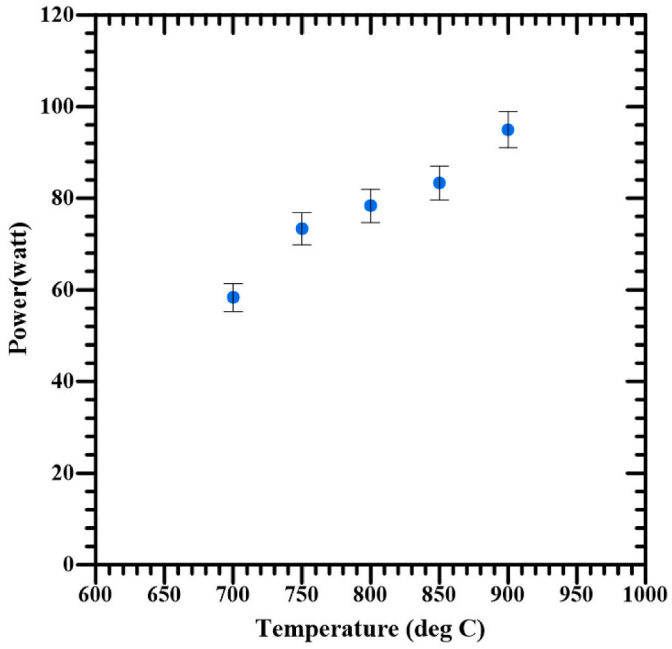

Fig. 13. Electric power of the SE versus the fluidized-bed temperature.

The performance of the SE was influenced by multiple interconnected factors, including the hydrogen pressure, fluidized-bed temperature, and cooling temperature. Because of the mutual interactions between these parameters, achieving the optimal power output P_{el} was challenging while adhering to limitations such as a low ash melting temperature and material temperature constraints that restricted the maximum fluidized-bed combustion temperature. Moreover, the temperature of the cold end depended on the temperature of the heat sink, which was approximately 25–30 °C in this study. The aforementioned limitations can be addressed through strategies such as reducing heat losses from exhaust gases and the outer surfaces of the burner and table, adjusting the cooling water system, and identifying further measures to maximize the SE's output.

The findings of this study confirm that the fluidized-bed combustion of mushroom waste, even on a small scale, is feasible for generating energy in an environmentally sustainable manner. The results of the experiments on the integrated SE and fluidized-bed reactor highlight the effectiveness of generating thermal or electrical energy from the sensible heat of the fluidizing gas. Such use of sensible heat makes a considerable contribution to the favorable $\eta_{overall}$ value of the designed CHP system. The successful integration of an SE with an FBC for biomass combustion to create a CHP system is a major advancement toward sustainable energy solutions. Stable combustion and consistent temperature profiles within the combustor of the designed system can be ensured using the optimized experimental conditions and by carefully controlling the air flow rate and biomass feed rate. The successful power generation achieved by the SE of the CHP system designed in this study validates this system's effectiveness in efficiently producing clean energy.

4.4. Gas emission results

The composition of the flue gas produced by combusting DMSW in the FBC was analyzed under biomass feeding rates and air flow rates of 50–60 L/min. The sand height in the fluidized bed was fixed at 2 cm. Flue gas samples were collected using a gas analyzer positioned at a height of 20 cm at the burner exit. Moreover, the gas temperature was measured using a K-type thermocouple. Each measurement was performed over a 10-min sampling period.

4.4.1. CO emissions

CO was primarily formed through devolatilization and primary reactions that occurred in the lower part of the FBC; the produced CO was then consumed in the postcombustion zones. CO is detected in flue gas if the combustion is incomplete (i.e., insufficient oxygen is available for converting carbon into CO_2), and factors such as inadequate mixing, low temperature, and short residence time contribute to the formation of CO.

The CO emissions of the designed fluidized-bed combustion system were primarily influenced by time, temperature, and turbulence. Because the mixing within the fluidized bed was effective, the need for multistage combustion was eliminated, thereby simplifying the system design. The aim of the proposed system design was to maximize the heat released within the fluidized bed. Flue gas analysis revealed that CO emissions tended to be higher at lower air ratios; however, the CO emission level typically remained below 300 ppm at 900 °C. The local minima in CO emissions occurred at favorable air ratios with high fuel input; thus, the optimal balance between residence time, combustion temperature, and turbulence was achieved under these parameters.

Fig. 14 displays the CO concentration during biomass combustion under different biomass feed rates and air flow rates. At an initial biomass feed rate of 9.5 g/min and an air flow rate of 60 L/min, the CO emission level was high because of the excess air present during combustion, which led to local flame quenching. As the feed quantity was increased, the carbon concentration gradually decreased by approximately 1000−230 ppm as the temperature of the FBC rose, thereby leading to more complete combustion and an increase in the CO_2 concentration. The CO emission levels of the proposed CHP system were considerably lower than the CO emission standard in Taiwan for stationary pollution sources (i.e., 2000 ppm at 6% O_2 [53]).

The CO emissions of the proposed design were reduced by adjusting the dimensions of its freeboard and horizontal cyclone to optimize the flow conditions.

4.4.2. NO emissions

NO is generated through the oxidation of nitrogen compounds in biomass fuel and air. In our experiments, we did not observe any thermal NO_x emissions between 800 and 900 °C. Fig. 15 depicts the NO emission profile of the designed system during biomass combustion under different air flow rates (50−60 L/min) and biomass feed rates (9.5–11 g/min). For all biomass feed rates, as the air flow rate was increased, the NO concentration increased. Notably, the highest NO concentration was observed at the feed rate of 9.5 g/min; this result was attributable to the use of LPG for preheating the sand under the aforementioned condition. However, a further increase in the feed rate caused the NO concentration to decrease gradually from approximately 240 to 130 ppm under an air flow rate of 60 L/min. The NO concentration then marginally increased again when the feed rate was further increased to 17 g/min. The aforementioned overall decreasing trend in the NO concentration was attributable to the devolatilization of DMSW during combustion, which resulted in the production of NH_3. The reaction of NH_3 with NO then led to the generation of N_2 and H_2O, which effectively inhibited the formation of nitrogen oxides. Notably, the NO emission levels of the proposed system were lower than the strict NO emission standards for solid fuel combustion in various regions of Taiwan (250 and 500 ppm at 6% O_2 [53]).

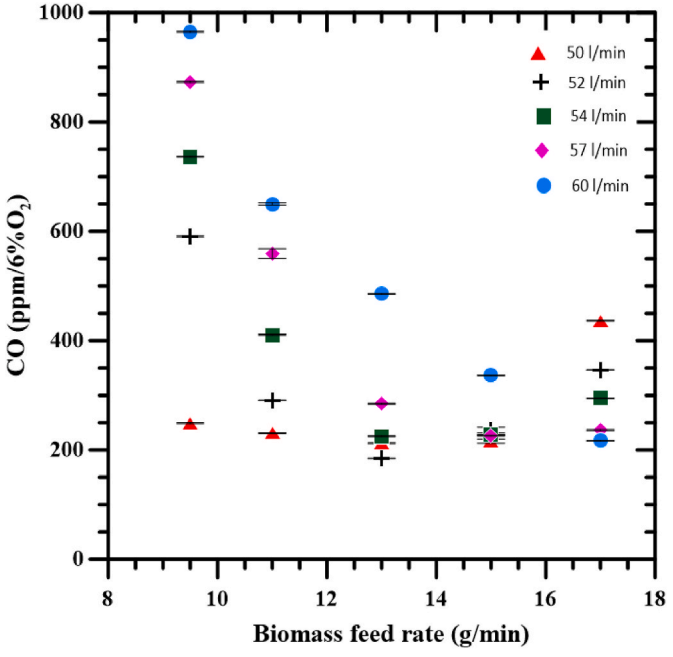

Fig. 14. Relationship between the biomass feed rate and the CO emissions of the designed CHP system.

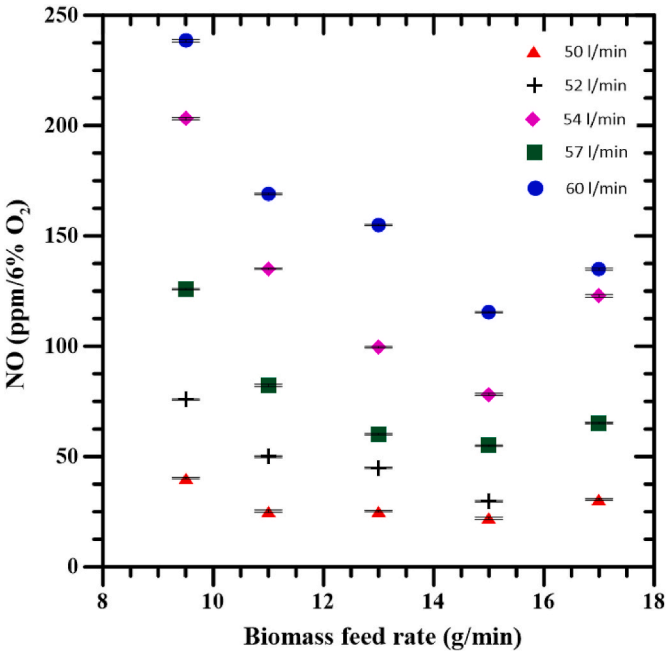

Fig. 15. Relationship between the biomass feed rate and the NO emissions of the designed CHP system.

4.4.3. O_2 emissions

Measuring the O_2 concentration after biomass combustion in a fluidized bed is essential for understanding the combustion process and its emissions. The O_2 concentration can be affected by the presence of CO and NO. Incomplete combustion, which is typically indicated by the presence of CO, results in a reduction in O_2 levels. When the oxygen available for complete combustion is insufficient, the carbon in the biomass partially oxidizes into CO rather than fully oxidizing into CO_2. Consequently, the O_2 levels in the flue gas decrease because some oxygen molecules are consumed in the formation of CO.

As the biomass feed rate was increased in this study, the O_2 concentration in the flue gas gradually decreased (Fig. 16), which indicated that a large quantity of fuel underwent oxidation within the fluidized bed and in the lower part of the combustor.

4.5. Comparison of the proposed system with relevant existing systems

Table 8 presents a comparison of the CHP systems developed in this study [28], and [49]. The thermal input to the system proposed in this study was considerably smaller than those to the other two systems;

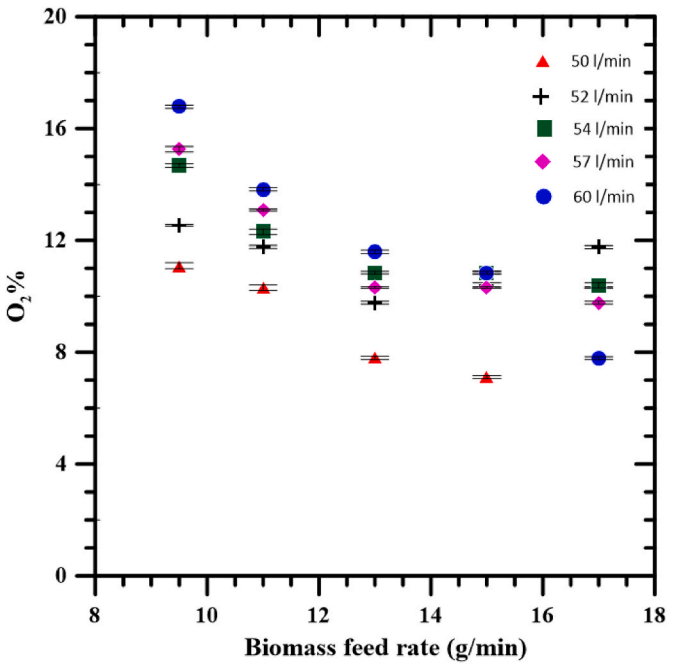

Fig. 16. Relationship between the biomass feed rate and the oxygen emissions of the designed CHP system.

Table 8
Comparison of the characteristics of the systems developed in the present study [28], and [49].

Literature		[49]	[28]	Present study
Stirling engine	Type	γ - configuration	α - configuration	γ - configuration
	Nominal electric power	500 W	5 kW	500 W
	Working fluid	N_2	He	H_2
	Pressure	4 & 8 bar	33 bar	2 bar
Biomass heat source	Design	Stationary fluidized bed	Stationary fluidized bed	Stationary fluidized bed
	Rated thermal input	20–23 kW	24–35 kW	2.7–4.8 kW
	Fuel	Wood pellets	Wood pellets	Discarded mushroom sawdust waste
Electrical power		272–547 W	3.8–4.8 kW	60–90 W
Thermal-to-Electrical efficiency		1.3–2.2 %	14–16 %	1.85–2 %
Fluidized bed temperature		745 °C–850 °C	800 °C	560 °C–900 °C
CO emissions (6% residual O_2)		<120 ppm	<470 ppm	<1000 ppm
NO_x emissions (6% residual O_2)		<120 ppm	–	<250 ppm

thus, the proposed system produced less electric power (90 W vs. 500 W and 5 kW). However, the η_e value of the proposed system was comparable to that of the system developed in Ref. [49] (2% vs. 2.2%). One major advantage of the proposed system over the other two systems is that it uses DMSW as fuel. Taiwan is estimated to produce 160,000 tons of DMSW every year; therefore, this biofuel is abundant and cheap. Consequently, the low η_e value of the proposed system is not a major issue. By contrast, the other two systems use wood pellets as fuel, and these pellets cost approximately 30 US dollars per 100 kg in Taiwan. Therefore, the revenue obtained through electricity generation must exceed the cost of this fuel by a sufficient margin for the aforementioned two systems to be economically viable. Another advantage of the proposed system is that the charge pressure of its SE is considerably smaller than those of the SEs of the other systems. Lower charge pressure results in lower stress on the mechanical components of the SE and causes fewer gas-leakage problems. In terms of emissions, the CO and NO_x levels of the proposed system are comparable to those of the other two systems and are well below the Taiwanese government's pollution standards.

5. Conclusion

In this study, a CHP system comprising an FBC and SE for biomass combustion was designed and experimentally evaluated. This system can produce electric power and heat energy from DMSW in an eco-friendly and sustainable manner. Because of the interconnected nature of the factors influencing the SE's performance, the Taguchi method was adopted for optimizing the experimental parameters to achieve optimal power generation while adhering to operational limitations. By carefully adjusting the SE's charge pressure, the fluidized-bed temperature, and the cooling temperature, we enhanced the power output and efficiency of the designed system. The results of this study confirm that the designed CHP system can be used to generate clean and renewable energy from DMSW in an economically feasible manner. The conclusions of this study are as follows.

1. The favorable heat transfer characteristics of the fluidized bed of the designed CHP system mean that the system can generate heat energy and electric power efficiently, and the SE of the system effectively recovers heat from the flue gas and converts this heat into electrical energy. Biomass fuels with various properties, including agricultural waste, can be used as the energy source of the designed system; thus, this system can generate heat and electricity in a sustainable and effective manner through biomass combustion.
2. Optimization of the biomass feed rate and air flow rate was found to considerably increase the combustion temperature. The results of this study provide valuable insights into methods for achieving higher combustion temperatures under favorable fluidization conditions in a CHP system. The SE's power output increased as the biomass feed rate was raised and the combustion temperature increased.
3. An increase in the biomass feed rate causes a decrease in the CO concentration in the flue gas of the designed system, which is attributable to biomass devolatilization. Furthermore, the results of this study highlight the importance of reducing heat losses for providing more heat to the SE.
4. Overall, the designed CHP system exhibits promising results for power generation and heat utilization, and its η_e value was discovered to be between 1.83% and 2.04%. Given that biomass waste is used as the fuel source in this system, such performance is satisfactory. Therefore, the aforementioned system can generate heat energy and electric power from biomass waste in an efficient and sustainable manner.
5. The designed system exhibited smooth, stable, and environmentally friendly operation in this study, which proves the feasibility of its practical application in the agricultural industry. This system can reduce the expenditure involved in biomass waste disposal and create additional revenue through electricity generation; thus, this system offers dual financial incentives for farm owners and investors.

The findings of this study contribute to the body of knowledge on CHP systems containing fluidized-bed biomass combustors and can be used for developing sustainable energy solutions. Future studies should conduct further research on and refine the experimental parameters of this study to develop biomass-based CHP systems with higher power generation efficiency and an expanded scope of application, thereby reducing the global reliance on fossil fuels and mitigating their environmental impacts.

CRediT authorship contribution statement

Wen-Lih Chen: Data curation, Formal analysis, Methodology, Writing – original draft. **Vadlakonda Sirisha:** Data curation, Formal analysis, Investigation. **Chi-Yuan Yu:** Conceptualization, Funding acquisition, Investigation, Project administration, Writing – original draft, Writing – review & editing, Supervision. **Yan-Ru Wang:** Data curation, Methodology. **Ming-Wei Dai:** Data curation, Methodology. **Janusz Lasek:** Funding acquisition, Project administration. **Yueh-Heng Li:** Conceptualization, Funding acquisition, Supervision, Writing – original draft, Writing – review & editing.

Declaration of competing interest

All authors declared that: (i) no support, financial or otherwise, has been received from any organization that may have an interest in the submitted work; and (ii) there are no other relationships or activities that could appear to have influenced the submitted work.

Data availability

Data will be made available on request.

Acknowledgments

This study was financially supported by the National Science and Technology Council of Taiwan (NSTC 112-2923-E-006-002-MY3; NSTC 112-2221-E-006-106) and the National Center for Research and Development in Poland (POLTAJ10/2022/49/MethaHydrAmmon).

Appendix

Calculation of thermal-to-electric efficiency and overall efficiency of the CHP system

The thermal-to-electric efficiency η_e of the designed CHP system was determined by evaluating the ratio of the electric power output generated by the system to its heat input. The relevant formula is as follows:

$$\eta_e = [\text{Electric power} / (\text{Biomass feed rate} \times \text{Specific heat of biomass})] \times 100,$$

where.

Electric power $= 90 - 100$ W,

Biomass feed rate $= 0.283$ g/s,

Specific heat of biomass $= 17.15$ kJ/g.

The electric power was within a range; therefore, the efficiency was calculated for the lower and upper bounds of the range. For the lower bound:

$$\eta_e = [90\ \text{W} \ / \ (0.283\ \text{g/s} \times 17.15\ \text{kJ/g})] \times 100 \approx 1.85\%.$$

For the upper bound:

$$\eta_e = [100\ \text{W} / (0.283\ \text{g/s} \times 17.15\ \text{kJ/g})] \times 100 \approx 2.04\%.$$

Therefore, the η_e of the designed system ranged from approximately 1.85%–2.03%.

The heat power generated by the designed CHP system was calculated as follows:

$$\textit{Heat power}\ (\text{W}) = \frac{\textit{Mass}_{water} \times C_{P,water} \times \left(T_{final} - T_{initial}\right)}{\textit{Time}}$$

$$= \frac{57\ \text{cm} \times 36\ \text{cm} \times 25\ \text{cm} \times 1\left(\frac{\text{g}}{\text{cm}^3}\right) \times 4.2\left(\frac{\text{J}}{\text{gK}}\right) \times 3\ (\text{K})}{10 \times 60(\text{s})} = 1077.3\ \text{J/s}\ (\text{W})$$

The overall efficiency $\eta_{overall}$ of the CHP for the maximum electric power is:

$$\eta_{overall} = \frac{\textit{Electric power} + \textit{Heat power}}{\textit{Input thermal power}} = \frac{100\ \text{W} + 1077\ \text{W}}{4853\ \text{W}} = 24.2\ \%$$

References

[1] Jiang Y, Asante D, Zhang J, Cao M. The effects of environmental factors on low-carbon innovation strategy: a study of the executive environmental leadership in China. J Clean Prod 2020;266:121998.
[2] Jiang Y, Zhang J, Asante D, Yang Y. Dynamic evaluation of low-carbon competitiveness(LCC) based on improved Technique for Order Preference by similarity to an Ideal Solution (TOPSIS) method: a case study of Chinese steelworks. J Clean Prod 2019;217:484–92.
[3] Li Y-H, Chuang B-C, Lin P-H, Lasek J. Effects of ammonia on combustion of coal in stoichiometric premixed methane–air flames. Fuel 2023;350:128825.
[4] Yu C-R, Cervera JA, Wu C-Y. Experimental study of the flame propagation of hydrogen - ammonia premixed fuels in porous media. Journal of Aeronautics, Astronautics and Aviation 2023;55(3):335–45.
[5] Wu C-Y. Numerical modeling of hydrogen catalytic reactions over a circular bluff body. Int J Hydrogen Energy 2022;47(88):37204–17.
[6] Li Y-H, Hsu H-W, Hsu H-W, Lien Y-S, Chao Y-C. Design of a novel hydrogen-syngas catalytic mesh combustor. Int J Hydrogen Energy 2009;34(19):8322–8.
[7] Li Y-H, Purwanto A, Chuang B-C. Micro-Explosion mechanism of iron hybrid Methane-Air premixed flames. Fuel 2022;325:124841.
[8] Li Y-H, Pangestu S, Purwanto A, Chen C-T. Synergetic combustion behavior of aluminum and coal addition in hybrid iron-methane-air premixed flames. Combust Flame 2021;228:364–74.
[9] Chou D, Tsai W-Y, Emami M-D, Li Y-H. Entropy Generation and Exergy Assessment of Methane-Nitrous Oxide Diffusion Flames in a Triple-Port Burner. Int J Energy Res 2023;2023:5364917.
[10] Chen C-H, Li Y-H. Role of N_2O formation of methane/nitrous oxide premixed flames. Combust Flame 2021;223:42–54.
[11] Li Y-H, Reddy SK, Chen C-H. Effects of the nitrous oxide decomposition reaction on soot precursors in nitrous oxide/ethylene diffusion flames. Energy 2021;235:121364.
[12] Chen G-B, Li Y-H, Cheng T-S, Chao Y-C. Chemical effect of hydrogen peroxide addition on characteristics of methane-air combustion. Energy 2013;55:564–70.

[13] Dimova-Cookson M, Stirk PMR. Multiculturalism and moral conflict. Routledge; 2009.
[14] Huang C-W, Li Y-H, Xiao K-L, Lasek J. Cofiring characteristics of coal blended with torrefied Miscanthus biochar optimized with three Taguchi indexes. Energy 2019; 172:566–79.
[15] Tong W, Liu Q, Ran G, Liu L, Ren S, Chen L, et al. Experiment and expectation: Co-combustion behavior of anthracite and biomass char. Bioresour Technol 2019;280: 412–20.
[16] Li Y-H, Chen H-H. Analysis of syngas production rate in empty fruit bunch steam gasification with varying control factors. Int J Hydrogen Energy 2018;43(2): 667–75.
[17] Kalak T. Potential use of industrial biomass waste as a sustainable energy source in the future. Energies 2023;16(4):1783.
[18] Abdalla AM, Hossain S, Azad AT, Petra PMI, Begum F, Eriksson SG, et al. Nanomaterials for solid oxide fuel cells: a review. Renew Sustain Energy Rev 2018; 82:353–68.
[19] Lasek J, Głód K, Słowik K, Cygan A, Li Y-H. Static and dynamic characteristics of rotary kiln reactor during processing of biomass and municipal solid waste. Powder Technol 2022;404:117476.
[20] Manatura K, Chalermsinsuwan B, Kaewtrakulchai N, Chao Y-C, Li Y-H. Co-torrefaction of rice straw and waste medium density fiberboard: a process optimization study using response surface methodology. Results in Engineering 2023;18:101139.
[21] Dong L, Liu H, Riffat S. Development of small-scale and micro-scale biomass-fuelled CHP systems – a literature review. Appl Therm Eng 2009;29(11):2119–26.
[22] Wu YT, Li YH. Combustion characteristics of a micro segment platinum tubular reactor with a gap. Chem Eng J 2016;304:485–92.
[23] Li YH, Wu CY, Lien YS, Chao YC. Development of a high-flame-luminosity thermophotovoltaic power system. Chem Eng J 2010;162(1):307–13.
[24] Li YH, Hong JR. Power generation performance of hydrogen-fueled micro thermophotovoltaic reactor. Int J Hydrogen Energy 2018;43(3):1459–69.
[25] Li Y-H, Li Y-H, Wu C-Y, Lien Y-S, Chao Y-C. Development of a high-flame-luminosity thermophotovoltaic power system. Chem Eng J 2010;162(1):307–13.
[26] Li Y-H, Wu C-Y, Li H-Y, Chao Y-C. Concept and combustion characteristics of the high-luminescence flame for thermophotovoltaic systems. Proc Combust Inst 2011; 33(2):3447–54.
[27] Li Y-H, Kao H-H, Wang Y-R, Wan J, Manatura K. Performance optimizing and entropy generation analysis of a platinum–stainless-steel segmented microreactor. Chem Eng J 2023;457:141151.
[28] Schneider T, Ruf F, Müller D, Karl J. Performance of a fluidized bed-fired Stirling engine as micro-scale combined heat and power system on wood pellets. Appl Therm Eng 2021;189:116712.
[29] Chen W-L, Huang C-W, Li Y-H, Kao C-C, Cong HT. Biosyngas-fueled platinum reactor applied in micro combined heat and power system with a thermophotovoltaic array and stirling engine. Energy 2020;194:116862.
[30] Chen W-L, Currao G, Li Y-H, Kao C-C. Employing Taguchi method to optimize the performance of a microscale combined heat and power system with Stirling engine and thermophotovoltaic array. Energy 2023;270:126897.
[31] Aberilla JM, Gallego-Schmid A, Azapagic A. Environmental sustainability of small-scale biomass power technologies for agricultural communities in developing countries. Renew Energy 2019;141:493–506.
[32] Obernberger I, Carlsen H, Biedermann F. Small-scale CHP plant based on a 35 kWel hermetic four cylinder stirling engine for biomass fuels-development, technology and operating experiences. Conference small-scale CHP plant based on a 35 kWel Hermetic Four cylinder Stirling engine for biomass fuels-development, technology and operating Experiences. Finnish Bioenergy Association.
[33] Vonžodas T. Research of factors influencing the burnout quality inside a biomass combustion chamber. Mechanics 2017;23(1):39–46.
[34] Yerbury A, Coote A, Garaniya V, Yu H. Design of a solar Stirling engine for marine and offshore applications. Int J Renew Energy Technol 2016;7(1):1–45.
[35] Laazaar K, Boutammachte N. New approach of decision support method for Stirling engine type choice towards a better exploitation of renewable energies. Energy Convers Manag 2020;223:113326.
[36] Thombare DG, Verma SK. Technological development in the Stirling cycle engines. Renew Sustain Energy Rev 2008;12(1):1–38.
[37] Demirbas A. Combustion characteristics of different biomass fuels. Prog Energy Combust Sci 2004;30(2):219–30.
[38] Piriou B, Vaitilingom G, Veyssière B, Cuq B, Rouau X. Potential direct use of solid biomass in internal combustion engines. Prog Energy Combust Sci 2013;39(1): 169–88.
[39] Lian Z, Wang Y, Zhang X, Yusuf A, Famiyeh L, Murindababisha D, et al. Hydrogen production by fluidized bed reactors: a quantitative perspective using the supervised machine learning approach 2021;4(3):266–87.
[40] Li YH, Kuo WC. The study of optimal parameters of oxygen-enriched combustion in fluidized bed with optimal torrefied woody waste. Int J Energy Res 2020;44(9): 7416–34.
[41] Klaren DG. Self-cleaning fluidised bed heat exchangers for severely fouling liquids and their impact on process design. In: Heat Exchangers-Basics design applications. IntechOpen; 2012.
[42] Gaderer M, Gallmetzer G, Spliethoff H. Biomass fired hot air gas turbine with fluidized bed combustion. Appl Therm Eng 2010;30(13):1594–600.
[43] Müller D, Plankenbühler T, Karl J. A methodology for measuring the heat release efficiency in bubbling fluidised bed combustors. Energies 2020;13(10):2420.
[44] Prima Z, Noda R. Agglomeration and Defluidization of silica sand and bentonite particles during empty fruit bunch (EFB) ash addition in bubbling fluidized bed (BFB) processes. J Chem Eng Jpn 2021;54(7):369–79.
[45] Dong H, Jiang X, Lv G, Chi Y, Yan J. Co-combustion of tannery sludge in a commercial circulating fluidized bed boiler. Waste Management 2015;46:227–33.
[46] Yliniemi J, Pesonen J, Tanskanen P, Peltosaari O, Tiainen M, Nugteren H, et al. Alkali activation–granulation of hazardous fluidized bed combustion fly ashes. Waste and biomass valorization 2017;8:339–48.
[47] Zhu S, Yu G, Liang K, Dai W, Luo E. A review of Stirling-engine-based combined heat and power technology. Appl Energy 2021;294:116965.
[48] Marra FS, Miccio F, Solimene R, Chirone R, Urciuolo M, Miccio M. Coupling a Stirling engine with a fluidized bed combustor for biomass. Int J Energy Res 2020; 44(15):12572–82.
[49] Urciuolo M, Chirone R, Saverio Marra F, Solimene R. Power generation by Stirling engine during fluidized bed combustion of wood pellets. Combust Sci Technol 2019;191(2):263–74.
[50] Chen G-L, Chen G-B, Li Y-H, Wu W-T. A study of thermal pyrolysis for castor meal using the Taguchi method. Energy 2014;71:62–70.
[51] da Silva Alves L, de Almeida Moreira BR, da Silva Viana R, Pardo-Gimenez A, Dias ES, Noble R, et al. Recycling spent mushroom substrate into fuel pellets for low-emission bioenergy producing systems. J Clean Prod 2021;313:127875.
[52] Ghani JA, Choudhury I, Hassan H. Application of Taguchi method in the optimization of end milling parameters. J Mater Process Technol 2004;145(1): 84–92.
[53] Standards for air pollutant emission from stationary pollution sources. Ministry of Environment; 2023.